



# Dynamically Tunable Terahertz Plasmon-Induced Transparency Analogy Based on Asymmetric Graphene Resonator Arrays

Bo Ni<sup>1</sup> · Guangsuo Tai<sup>1</sup> · Haibin Ni<sup>1</sup> · Lingsheng Yang<sup>1</sup> · Heng Liu<sup>1</sup> · Lingli Huang<sup>2</sup> · Jiang Wang<sup>3</sup> · Jianhua Chang<sup>1</sup>

Received: 12 May 2021 / Accepted: 27 August 2021 / Published online: 17 September 2021  
© The Author(s), under exclusive licence to Springer Science+Business Media, LLC, part of Springer Nature 2021

## Abstract

A plasmon-induced transparency (PIT) effect based on an asymmetric graphene loop structure has been proposed and investigated in this paper. The microstructure consists of a pair of graphene square loops and a dielectric substrate. The calculated results show that the transparency peak can be produced at 5.68 THz by the frequency detuning between two different graphene square loops. The geometric parameters of microstructure, such as the coincidence degree between two square loops, the length and the width of two square loops, will affect the position of PIT-window. Moreover, by adjusting the Fermi level of graphene through external gate voltage, the PIT-window can be dynamically tuned. Importantly, the PIT-window in graphene metamaterials can also serve as the amplitude modulator at the fixed frequency and the refractive index sensor. In addition, an improved microstructure is proposed for realizing the multi-PIT-window. The amplitude modulation of multi-PIT-window can be adjusted up to 53% by controlling the coupling distance, which has certain application prospects in the fields of double-channel filters, optical switches, and modulators.

**Keywords** Terahertz graphene metamaterials · Active tunability · Plasmon-induced transparency · Multi-PIT-window

## Introduction

Since electromagnetically induced transparency (EIT) effect was originally observed in the atomic system, it has been attracting the attention of researchers [1, 2]. EIT effect is often accompanied by strong dispersive and slow-light property, which can be employed in slow-light devices [3], optical switches [4], filters [5], and sensors [6, 7]. Metamaterial is a kind of artificial periodic composite material, which can be widely applied in photodetectors [8, 9], optical polarizers [10], and perfect absorbers [11]. Recent discoveries have found that plasmon-induced transparency (PIT) effect

can also be realized in the metamaterial structures, which is the classic analogy of EIT-like effect based on various coupling principles [12]. PIT effect in metamaterials can not only effectively avoid the strict experiment conditions, but also take advantage of the unique properties of metamaterials. Generally, four main kinds of schemes can be adopted to realize the PIT effect: bright-bright mode coupling [13], bright-dark mode coupling [14], phase coupling [15], and bright-quasi dark mode coupling [16]. Zhang et al. proposed a metal metamaterial structure with near-field coupling between bright and dark modes to achieve the EIT-like effect [17]. Meng et al. experimentally verified polarization-independent PIT effect through bright-dark mode coupling between split-ring and spiral-ring [18]. Liu et al. designed a three-dimensional metamaterial structure and theoretically analyzed the formation reason for PIT effect [19]. Additionally, Jin et al. theoretically demonstrated the PIT effect based on bright-bright mode coupling by two silver strips [20]. The bright-bright mode coupling can be directly excited by incident plane waves to produce PIT-window, which depends on the weak hybridization caused by the frequency detuning, while the bright-dark mode coupling mainly relies on the destructive interference between two modes [21]. So far, many PIT effect in metamaterials have been proposed in the

✉ Bo Ni  
bni@nuist.edu.cn

<sup>1</sup> Jiangsu Key Laboratory of Meteorological Observation and Information Processing, School of Electronic and Information Engineering, Nanjing University of Information Science & Technology, Nanjing 210044, China

<sup>2</sup> School of Lifelong Education, Nanjing University, Nanjing 210093, China

<sup>3</sup> School of Microelectronics and Control Engineering, Changzhou University, Changzhou 213164, China

grating structure [22], resonators and planar structure [23], and waveguide structure [24]. However, these structures are mostly composed of metal materials. Due to the shortcomings of material loss in metals and its determined structure, it is difficult to change its structural parameters, which greatly restricts the practical application of PIT effect.

At present, the researchers have attempted to realize the tunable PIT effect by simple metamaterial structures, such as MEMS technology [25], electrical operations [26], thermal control [27], and photosensitive materials [28]. Among them, graphene has attracted considerable attention due to its properties of electrical controllability. Graphene is a honeycomb-shaped two-dimensional structure with the thickness of only about 0.34 nm [29]. The surface conductivity of graphene can be adjusted by applying the gate voltage or chemical doping, which is very helpful for dynamic tunability of electromagnetic response. Thus, some dynamically tunable PIT effects in graphene metamaterials have been proposed. Chen et al. designed a system of tunable PIT effect based on the near-field bright-dark mode coupling by graphene nanostrips [30]. Zhang et al. demonstrated a  $\Pi$ -shaped graphene structure with the adjustable broadband PIT-window [31]. Ning et al. obtained a multi-band PIT-window by using the composite structure with graphene films and air grooves [32]. Nowadays, the tunable multiple PIT effect is becoming a new trend for researchers and the results above demonstrate that graphene is an ideal option for realizing the tunable single and multiple PIT effect.

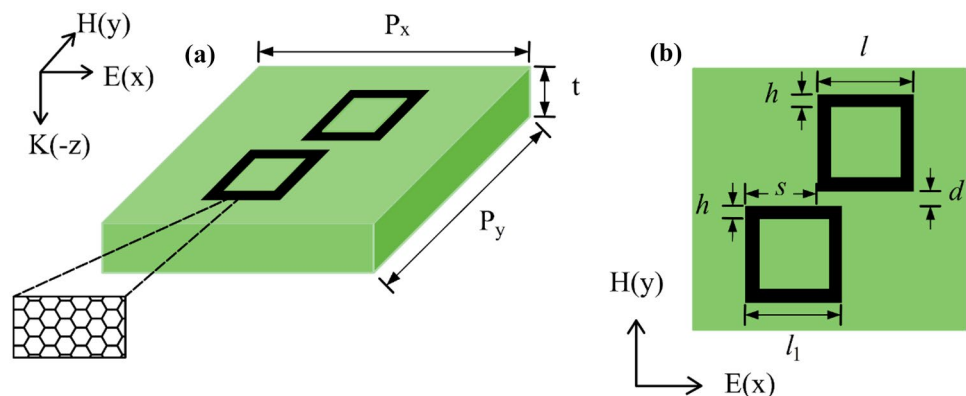
In this paper, firstly, we propose an asymmetrical graphene loop structure to realize the dynamically tunable PIT effect. The structure mainly consists of two graphene square loops (two-dimensional materials) and a quartz dielectric substrate. This microstructure adopts the method of bright-bright mode coupling. When incident light is irradiated on the microstructure, two graphene square loops with different structural parameters can be excited at the same time. When the distance between two square loops and the lateral offset is appropriate, the frequency detuning between the two graphene square loops will cause the weak hybridization, which

results in a sharp PIT-window. Meanwhile, the influence of structural and environmental parameters on the PIT-window have been studied, such as the width of two graphene square loops, the length of single square loop, the lateral offset between two square loops, and the refractive index of substrate. The Fermi level of graphene can also be controlled to change the position of PIT-window. The variation of transmission spectrum with different Fermi levels is also considered, when the Fermi level of each graphene square loop is independently controlled. Additionally, an improved graphene microstructure is proposed to realize the multi-PIT-window, and the amplitude modulation of multi-PIT-window can reach up to 53%. Obviously, the simple planar structure can be widely used in many fields such as multi-channel filters, optical switches, modulators, and sensors.

### Structure Description and Theoretical Model

Figure 1 a and b respectively show a three-dimensional and top view of the microstructure. The microstructure is divided into two layers: the upper layer is a graphene layer, and the lower layer is a quartz substrate with a dielectric constant of 2.6. The thickness of dielectric substrate  $t$  is 1  $\mu\text{m}$ . By using the finite-difference time-domain (FDTD) method, the graphene microstructure can be numerically simulated. In terms of setting simulation parameters,  $X$ - and  $Y$ - directions can be set as periodic boundary conditions, and  $Z$ -direction can be set as PML boundary conditions. The incident plane light is along the  $Z$ -direction, and its polarization direction ( $E$ ) is parallel to the  $X$ -direction. In aspects of the structural parameters of graphene loops, the lengths of two square graphene loops are  $l = 1300$  nm and  $l_1 = 1200$  nm, the width of the two square loops  $h$  is 320 nm, and the lateral offset between two square loops  $s$  is 600 nm. The Fermi level of graphene is set as 0.65 eV, and the distance between the two square loops  $d$  is set as 600 nm. The length of periodic substrate is 4  $\mu\text{m}$  in both  $X$ - and  $Y$ -directions. Among all of them, the lateral offset  $s$ , the length of the square loop  $l$  and the spacing between two loops  $d$  are all variable.

**Fig. 1** **a** Three-dimensional view of graphene loop microstructure. **b** Top-view of graphene loop microstructure



Generally speaking, the total conductivity of graphene is composed of intra-band conductivity  $\sigma_{\text{inter}}$  and inter-band conductivity  $\sigma_{\text{intra}}$  when the Fermi level of graphene is greater than half of the photon level, according to the Pauli blocking principle [33], the inter-band transition can be ignored, and the conductivity of graphene is mainly determined by the intra-band transition. The photon level in the terahertz (THz) band is quite low and the conditions are very simple to satisfy. Therefore, the intra-band conductivity  $\sigma_{\text{intra}}$  can be equal to the total conductivity in the THz band. The simulation waveband of this structure is 4–8 THz. When the surface conductivity of graphene is described by the Drude model, it satisfies the following formula [34, 35]:

$$\sigma_{\text{total}} = \sigma_{\text{intra}} + \sigma_{\text{inter}} \tag{1}$$

where

$$\sigma_{\text{intra}} = \frac{2e^2k_B T}{\pi h^2} \ln \left[ 2 \cosh \left( \frac{E_f}{2k_B T} \right) \right] \frac{i}{\omega + 2\Gamma} \tag{2}$$

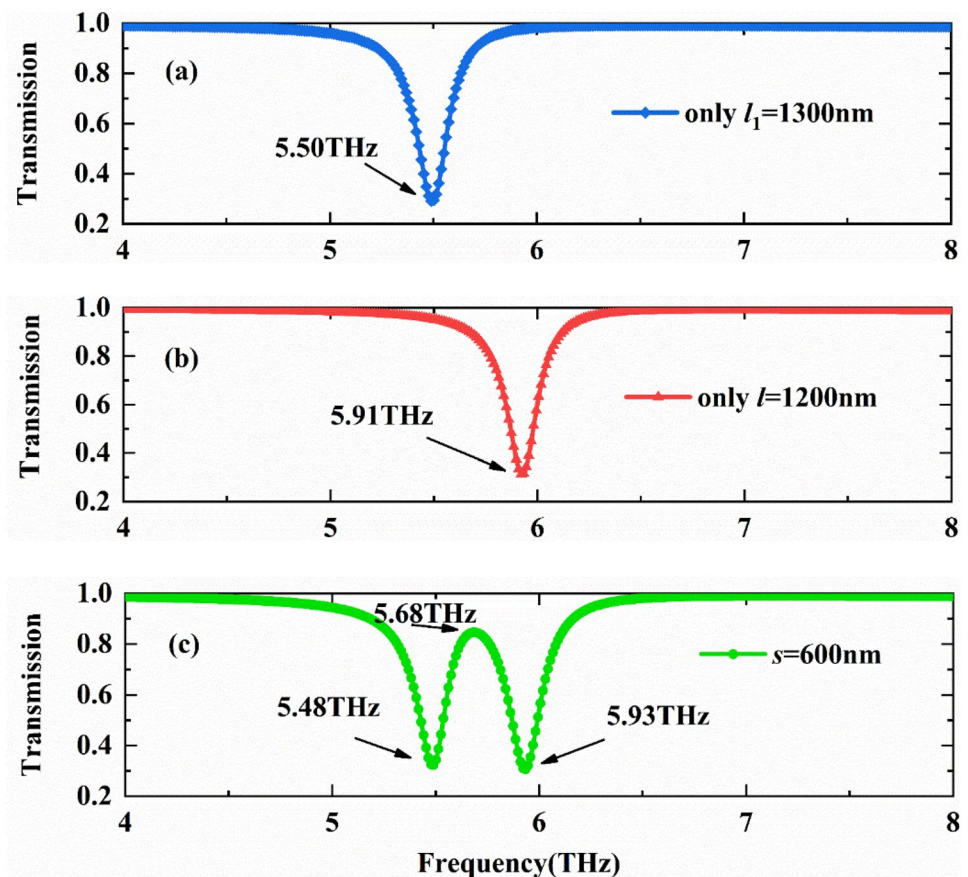
$$\sigma_{\text{inter}} = \frac{e^2}{4h} \left[ \frac{1}{2} + \frac{1}{\pi} \arctan \left( \frac{h\omega - 2E_f}{2k_B T} \right) - \frac{i}{2\pi} \ln \left( \frac{(h\omega + 2E_f)^2}{(h\omega - 2E_f)^2 + (2k_B T)^2} \right) \right] \tag{3}$$

Where in  $E_f$  represents the Fermi level of grapheme,  $k_B$  denotes the Boltzmann constant,  $\omega$  is the angular frequency,  $\hbar$  is the reduced Planck constant,  $T=300\text{ }^\circ\text{C}$  is the temperature, and  $\Gamma=0.21\text{ meV}$  represents the carrier scattering rate. In addition, when the width of the graphene loop  $h$  is greater than 30 nm, the edge-quantum-confined effect can be ignored [36]. The Fermi level of graphene can be changed by applying an external gating voltage, and thus, the conductivity of graphene can be dynamically adjusted.

### Results and Discussions

Figure 2 shows the transmission spectrum of separate graphene square loop and combined graphene loop structure excited by the incident plane wave, when the structural parameters are stable: the lateral offset  $s$  is 600 nm, the spacing between loops  $d$  is 600 nm, and the chemical

**Fig. 2** **a** Transmission spectrum of square graphene loop II when singly excited. **b** Transmission spectrum of square graphene loop I when singly excited. **c** Transmission spectrum of two combined square graphene loops when simultaneously excited



potential of graphene  $E_f$  remains 0.65 eV. Due to the electric field direction of incident plane wave is along the  $X$ -direction, two separate graphene square loops can both be directly excited to produce electromagnetic resonance. Two graphene square loops can respectively produce obvious transmission valleys at 5.50 THz and 5.91 THz, so they can be considered to act as bright model, as shown in Fig. 2a, b. When the combined graphene square loops  $l$  and  $l_1$  are placed along the vertical direction and the polarization direction of electric field is along the  $X$ -direction, an obvious PIT-window can be observed at 5.68 THz, as shown in Fig. 2c. The two transmission valleys are located at 5.48 THz and 5.93 THz, respectively, which are slightly shifted from the original resonance frequency. By comparing with the simulation and experimental results of previous literatures [20, 37, 38], the appearance of PIT-window in the spectral response of our proposed structure is consistent with the spectral characteristics of classical EIT analogue by the hybridization between two bright modes.

Furthermore, to better understand the formation mechanism of PIT-window, we study the total electric field distribution diagram  $|E|$  and the  $Z$ -direction distribution of electric field diagram  $E_z$ , when the structural parameters of graphene loop structure are stable ( $s = 600$  nm,  $d = 600$  nm), as shown in Fig. 3.

According to Fig. 3a–c, the surface total electric field is generally distributed on the inner and outer sides of graphene square loops, which is similar to the electric field distribution of a typical electric dipole oscillation. The square graphene loop  $l_1$  can be excited by incident light at the frequency of 5.93 THz, while the square graphene loop

$l$  is hardly excited, as shown in Fig. 3a. As can be observed from Fig. 3c, when the frequency is 5.48 THz, the square graphene loop  $l$  is strongly excited, and the square graphene loop  $l_1$  can be only weakly excited. At the frequency of 5.68 THz, two combined graphene square loops can be excited at the same time. The total electric field intensity of combined graphene square loops is weaker than the electric field intensity excited separately, as depicted in Fig. 3b.

In addition, by observing the  $Z$ -direction distribution of electric field  $E_z$ , the reason for the appearance of narrow PIT-window can be further interpreted. At the frequency of two transmission valleys, the resonance direction of induced electric field of two separate square loops is consistent, as shown in Fig. 3d, f. At the frequency of transmission peak, the resonance direction of induced electric field of two combined square loops is opposite. As a result, the quadrupole resonance and frequency detuning caused by the strong near-field coupling leads to the PIT effect, as shown in Fig. 3e.

Moreover, Fig. 4 shows the influence of lateral offset  $s$  on the PIT-window when the length  $l_1$ ,  $l$ , and the spacing  $d$  of two square graphene loops are stable. Obviously, the lateral offset  $s$  determines the coupling strength between two graphene loops. When the lateral offset  $s$  increases from 0 to 600 nm, the lower the coincidence degree of two square loops becomes, the more balanced the strength of coupling between two square loops tends to be. When  $s$  is 600 nm, the induced electric field intensity of two square loops is at a comparable level, and the frequency detuning can be easily achieved, which can result in a more obvious PIT-window. After  $s$  exceeds 600 nm, the difference between two square

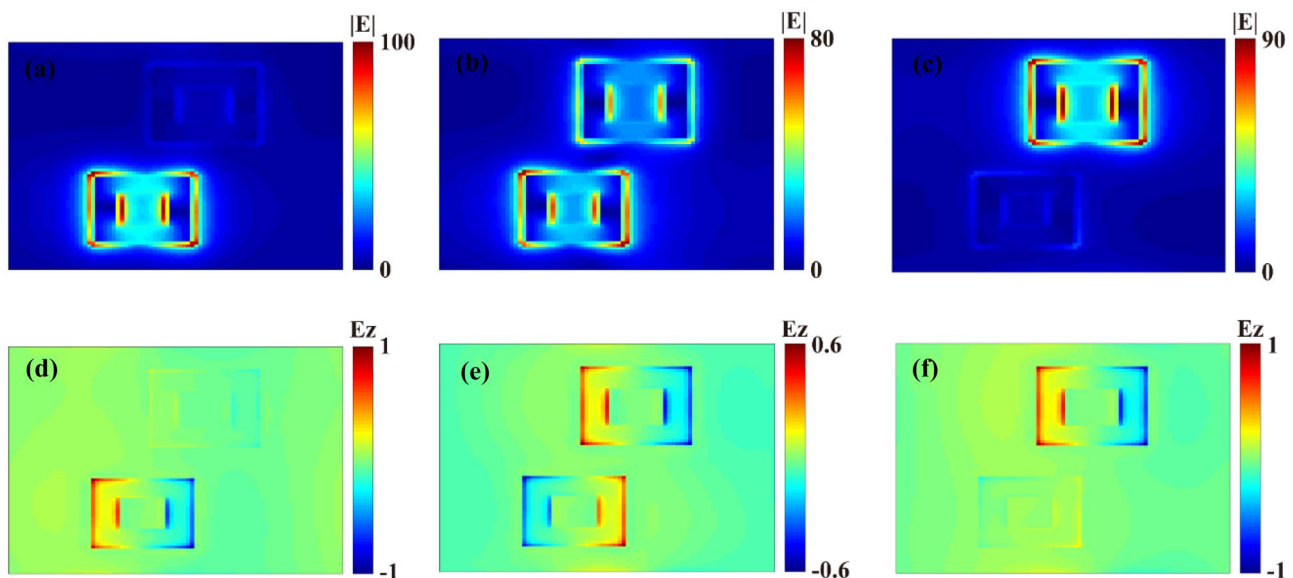


**Fig. 3** Total electric field diagram at the frequency of **a** 5.93 THz, **b** 5.68 THz, and **c** 5.48 THz.  $Z$ -direction distribution of electric field at the frequency of **d** 5.93 THz, **e** 5.68 THz, and **f** 5.48 THz

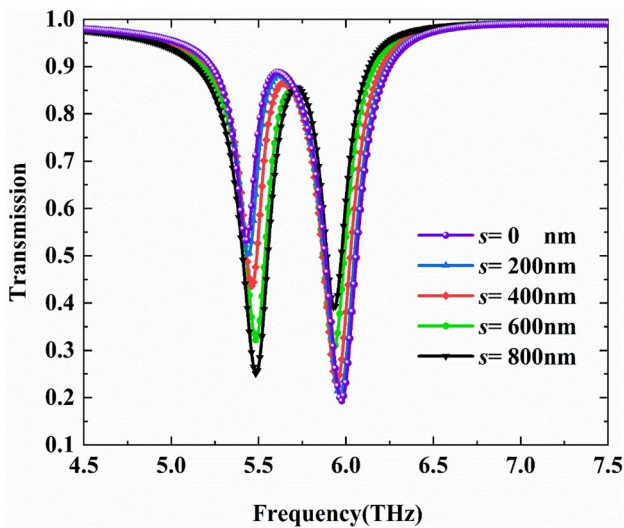


**Fig. 4** Transmission spectrum with the lateral offset  $s$  changing ( $d=600$  nm,  $l=1300$  nm,  $l_1=1200$  nm)

loops’ induced electric field intensity increases, which will lead to the deformation of PIT-window.

Figure 5 demonstrates the variation of transmission spectrum with the width  $h$  of square loops  $l$  and  $l_1$  increasing, when keeping the lateral offset  $s$  between graphene loops  $l$  and  $l_1$  unchanged. When the loop’s width  $h$  increases from 220 to 370 nm, the amplitude of transmission peak remains about 0.85, and PIT-window will blue-shift, owing to the change of electromagnetic resonance frequencies of two graphene loops. At the same time, the depth of transmission valley will be furtherly deepened because the intensity of

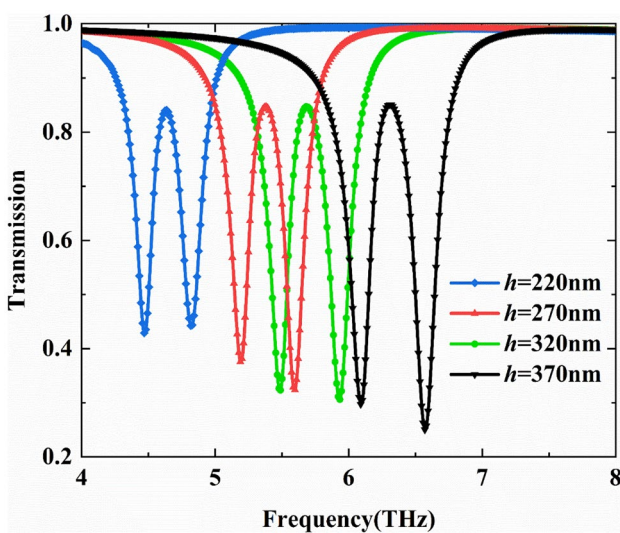


**Fig. 5** Transmission spectrum with the width of graphene loops  $h$  changing ( $s=600$  nm,  $l=1300$  nm,  $l_1=1200$  nm)

each graphene square loop’s electromagnetic resonance will also strengthen, with the width  $h$  of square loops increasing.

Also, we study the influence of square loop’s length  $l$  on the PIT-window when other structural parameters remain unchanged. As shown in Fig. 6, when the length  $l$  and  $l_1$  are both 1200 nm, only a deep transmission valley appears because two square loops have the same resonance mode. As the length  $l$  increases from 1200 to 1500 nm, the position of transmission valley of square loop  $l_1$  remains unchanged. Meantime, the position of transmission valley of square loop  $l$  will red-shift. Due to the difference between two square loops’ resonant frequency increases, the near-field coupling strength will become weaker, which leads to the expansion of PIT-window.

Besides, the surface conductivity of graphene metamaterials depends on its Fermi level. The Fermi level can be adjusted by chemical doping or applying an external bias voltage. On the one hand, the Fermi level affects the resonance frequency of graphene. Figure 7 shows the transmission spectrum with different Fermi levels when the overall parameters of structure remain unchanged. With the Fermi energy continuously increasing from 0.55 to 0.85 eV, the PIT-window has a blue-shift, and satisfies the conclusion  $f \propto \sqrt{kE_f} / 2\pi^2 hcl$  [39], where  $f$  is the resonant frequency of structure,  $k = e^2 / hc$  is a fixed structural constant, and  $l$  is the length of graphene loop. On the other hand, when the Fermi level  $E_f$  keeps stable, as the length of graphene loop  $l$  continues to increase from 1200 to 1500 nm, the resonance frequency of graphene loop becomes red-shifted, which satisfies the variation trend of the resonant frequency of square loop  $l$ , as shown in Fig. 6. Thus, PIT-window in graphene

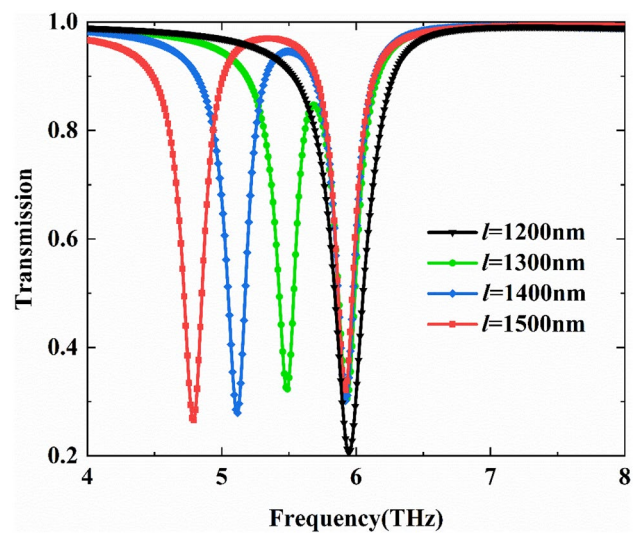


**Fig. 6** Transmission spectrum with the length of square loop  $l$  changing ( $l_1=1200$  nm,  $d=600$  nm,  $s=600$  nm)

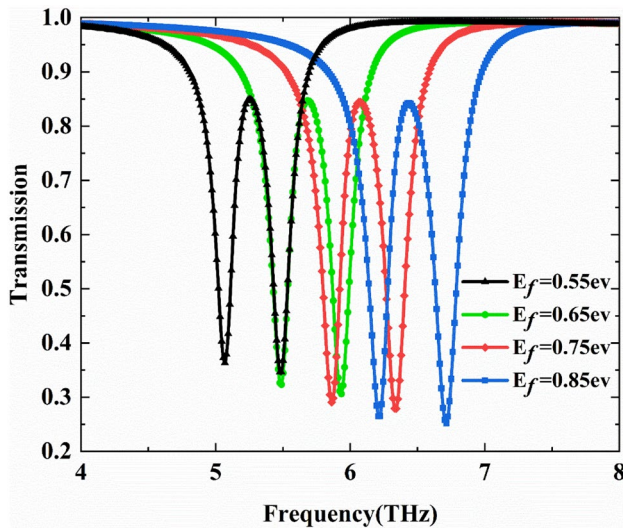


**Fig. 7** Transmission spectrum with different Fermi levels ( $l = 1300$  nm,  $ll = 1200$  nm,  $d = 600$  nm,  $s = 600$  nm)

metamaterials can become adjustable, which avoids the disadvantages of metal materials that need to modify the geometric parameters of microstructure.

Ideally, the Fermi level of each graphene square loop can be independently controlled; thus, our proposed graphene square loop microstructure can dynamically adjust the amplitude of transmission peak at a fixed frequency. As depicted in Fig. 8, when the Fermi level of two graphene loops are  $E_{fl} = 0.6$  eV and  $E_{fr} = 0.7$  eV, only a transmission valley appears at the frequency of 5.7 THz because two square loops have the same resonance frequency. When  $E_{fl}$

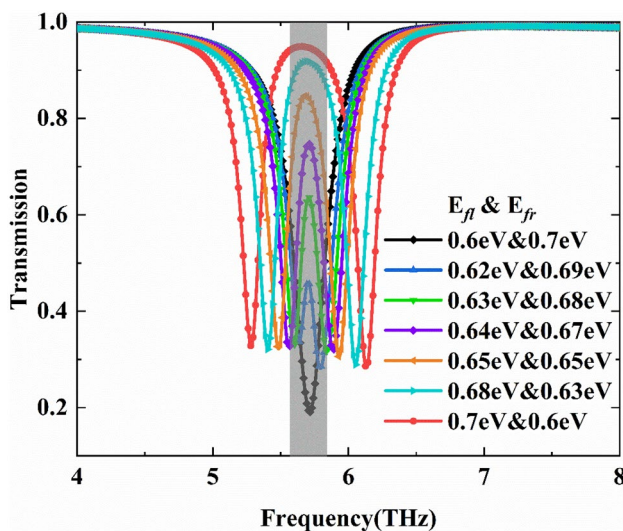


**Fig. 8** Transmission spectrum at the fixed frequency of 5.7 THz with different Fermi levels  $E_{fl}$  and  $E_{fr}$

**Table 1** The amplitude of transmission peak at the fixed frequency of 5.7 THz with different Fermi levels  $E_{fl}$  and  $E_{fr}$

$E_{fl}$ (eV)	$E_{fr}$ (eV)	Transmission peak frequency (THz)	Transmission peak amplitude
0.6	0.7	5.7	0.19
0.62	0.69	5.7	0.46
0.63	0.68	5.7	0.63
0.64	0.67	5.7	0.74
0.65	0.65	5.7	0.84
0.68	0.63	5.7	0.91
0.7	0.6	5.7	0.95

increases from 0.6 to 0.7 eV and  $E_{fr}$  decreases from 0.7 to 0.6 eV, the PIT-window will gradually appear and the width of PIT-window tends to expand. At the same time, the transmission peak remained at the frequency of about 5.7 THz. For the microstructure at different Fermi levels ( $E_{fl}$  and  $E_{fr}$ ), the amplitude of transmission peak at the fixed frequency of 5.7 THz is listed in Table 1. By applying different bias voltages to two graphene square loops, the amplitude modulation depth of modulator  $T_M$  ( $T_M = |T_{Max} - T_{Min}| / T_{Max}$ ) can reach up to 80%. Therefore, the microstructure can also act as an amplitude modulator or optical switch with electric tuning in the terahertz region.

The sensitivity of our proposed microstructure as a refractive index sensor is also considered. Figure 9 shows the variation of transmission spectrum with the refractive index (RIU) of medium substrate changing. As shown in Fig. 9, when the substrate RIU increases from 1.2 to 1.8, the PIT-window will have a red shift, and the transmission peak

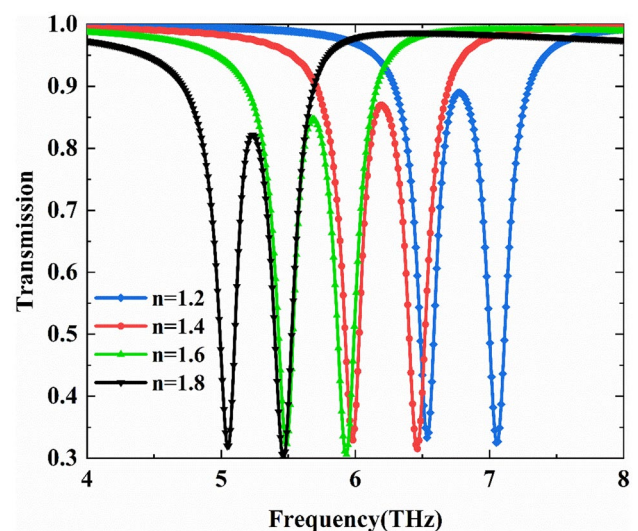


**Fig. 9** Transmission spectrum with different refractive indexes of medium substrate

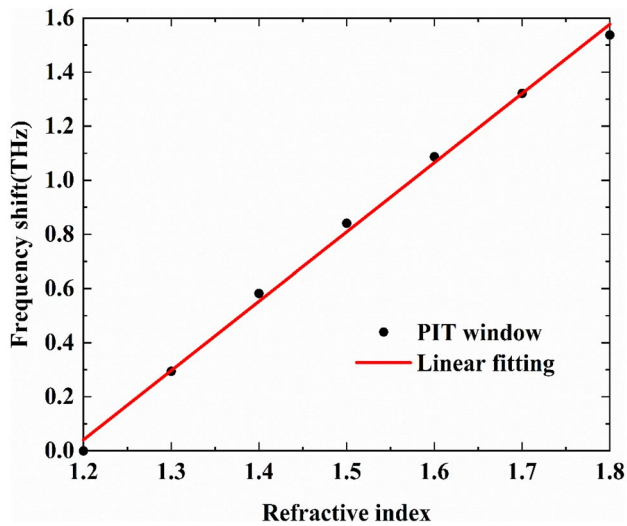


**Fig. 10** Fitting function of PIT with different substrate refractive index. Multi-PIT-window structure model and results analysis

has moved from 6.77 to 5.23 THz. The slope obtained by fitting the curve is about 2.57 THz/RIU, which can satisfy the sensitivity requirements of refractive index sensor. The data fitting curve is shown in Fig. 10, and the linear fitting is in line with expectation.

In this section, an improved composite graphene resonator structure is proposed to realize the multi-PIT-window. Figure 11 shows the top view of structure. As depicted in Fig. 11, a graphene strip with appropriate spacing is placed between two square loops so that the resonance frequency of graphene strip is close to the resonant frequency of two

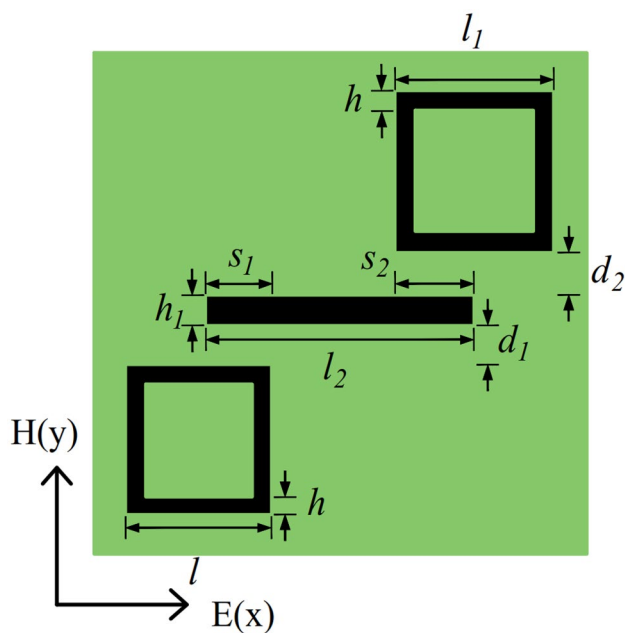


**Fig. 11** Top view of composite graphene microstructure

graphene square loops, thereby generating a multi-PIT-window by bright-bright-bright mode coupling.

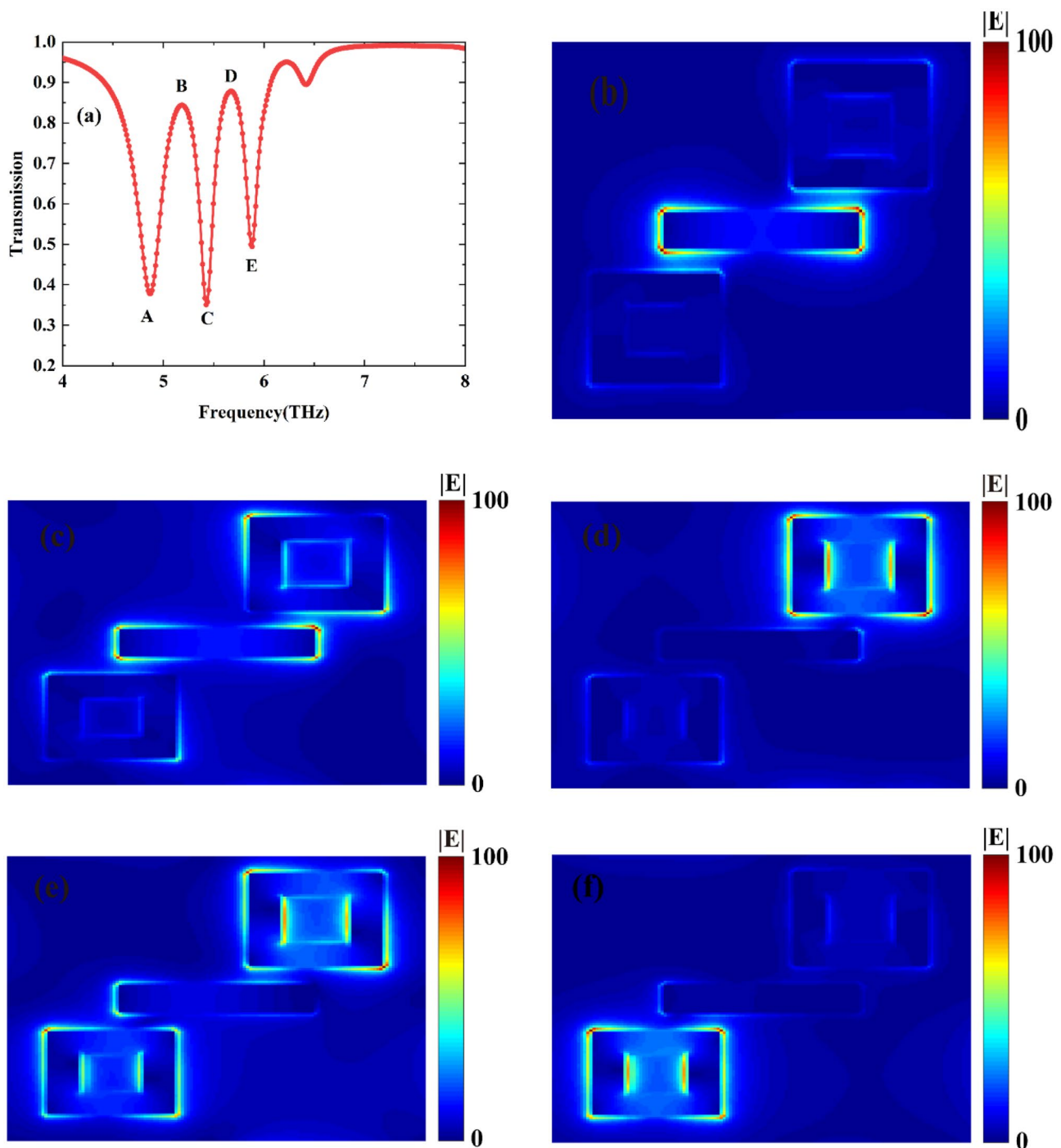
The structural parameters of two graphene square loops remain unchanged ( $l = 1300$  nm,  $l_1 = 1200$  nm,  $h = 320$  nm), the length of graphene strip  $l_2$  is 1900 nm, the width  $h_1$  is 400 nm, the lateral offset between the left square loop and graphene strip  $s_1$  is 550 nm, the lateral offset  $s_2$  between the right square loop and graphene strip is 650 nm, and the coupling distances  $d_1$  and  $d_2$  between two graphene square loops and central graphene strip are both 150 nm. The incident plane wave is still along the Z-direction, and the polarization direction of the electric field is set along the X-direction. The Fermi level of graphene strip and square loops is both set as 0.65 eV.

Figure 12a shows the transmission spectrum of composite graphene structure and an obvious multi-PIT-window can be observed. The resonance frequencies at the point B and D are  $f_B = 5.14$  THz and  $f_D = 5.68$  THz. As shown in Fig. 12a, the amplitude of two transmission peaks B and D can reach up to 0.85 and 0.87, respectively. Both the graphene square loops and graphene strip can be directly excited by the incident light because the polarization direction of incident plane wave is along the X-direction. The resonance frequencies at the points A, C, and E are  $f_A = 4.85$  THz,  $f_C = 5.45$  THz, and  $f_E = 5.87$  THz, which exhibits the characteristics of three bright modes in the transmission spectrum.

In order to understand the formation mechanism of multi-PIT-window, we observe the total electric field distribution  $|E|$  at the point of A–E, as shown in Fig. 12b–f. According to Fig. 12b, d, and e, the graphene strip and graphene square loops are respectively excited by the incident wave at the point of A, C, and E, surface electric field  $|E|$  mainly distribute at both ends of graphene loops and strip, and electric field of other parts can nearly be neglected.

As shown in Fig. 12c, the total electric field diagram at the point of B is localized at the graphene strip and square loop  $l$ , which indicates that the transmission peak B is generated by the frequency detuning between the graphene strip and square loop  $l$ , and the square loop  $l_1$  is hardly excited. As depicted in Fig. 12e, the transmission peak D is not just caused by the frequency detuning between two graphene square loops. In addition to the obvious electric field distribution at two graphene square loops which can be observed, the left side of graphene strip also has an intense surface electric field. Therefore, the joint coupling between graphene strip, square loop  $l$ , and square loop  $l_1$  contributes to the transmission peak D.

Finally, we have studied the influence of coupling distance  $d_1$  and  $d_2$  on the multi-PIT-window, as shown in Fig. 13. As the coupling distance  $d_1$  and  $d_2$  decreases, the coupling strength between the graphene square loop  $l_1$  and strip becomes stronger. Therefore, the first PIT-window tends to be more and more obvious with the coupling distance



**Fig. 12** **a** Transmission spectrum of composite graphene structures. Total electric field distribution diagram with different frequencies of incident wave: **b** 5.17 THz (point A), **c** 5.34 THz (point B), **d** 5.46 THz (point C), **e** 5.71 THz (point D), **f** 5.92 THz (point E)

$d_1$  and  $d_2$  decreasing. When the coupling distance  $d_1$  and  $d_2$  changes within a certain range, the amplitude of transmission peak  $D$  varies slightly. By controlling the coupling distance  $d_1$  and  $d_2$ , the position and amplitude of first PIT-window can be easily controlled, and the position of second EIT-window can be stable at the same time. The improved

structure can be applied to multi-channel filters and modulators. The performance of modulation can be evaluated by the amplitude modulation depth of transmission peak ( $T_M$ ), which is defined as  $T_M = |T_{\text{Max}} - T_{\text{Min}}|/T_{\text{Max}}$  [40]. It can be calculated that the maximum amplitude modulation depths for transmission peak is about 53%.



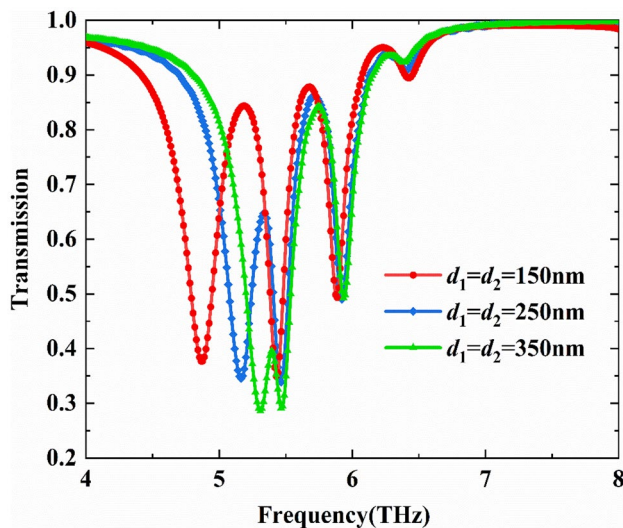


**Fig. 13** The transmission spectrum with different coupling distances  $d_1$  and  $d_2$

## Conclusion

In this paper, we make use of an asymmetric graphene loop structure to achieve the tunable PIT-window in the terahertz region through the bright-bright mode coupling. At the same time, the simulation results show that the parameters of microstructure also have a great impact on the PIT-window. Importantly, when the Fermi level of graphene increases from 0.55 to 0.85 eV, the PIT-window will totally be blue-shifted, which can effectively control the position of PIT-window. In addition, the amplitude of transmission peak at the fixed frequency of 5.7 THz can be tuned from 0.19 to 0.95 and the amplitude modulation depth can reach up to 80%, when the Fermi levels of two graphene loops with different values change accordingly. Our proposed microstructure also has a sensitivity of 2.57 THz/RIU to the variation of substrate's refractive index. Finally, we propose a composite structure to realize the multi-PIT-window, and the multi-PIT-window can also be effectively adjusted by controlling the Fermi energy of graphene. The multi-PIT-window is sensitive to the coupling distance, and the amplitude of transmission peak can be adjusted through the coupling distance. The amplitude modulation can reach up to 53%. Therefore, the single and multiply PIT-window realized in the terahertz band can obtain certain application prospects in multi-channel filters, optical switches, amplitude modulators, and sensors.

**Author Contribution** All authors contributed to this work.

**Funding** This work was supported by the National Natural Science Foundation of China under Grant 61875089, the National Natural Science Foundations of China under Grant 61705021 and the Kunshan and Nanjing University of Information Science and Technology (NUIST) intelligent sensor research center project.

**Availability of Data and Material** The datasets analyzed during the current study are available from the corresponding author on reasonable request.

## Declarations

**Ethics Approval** Not applicable.

**Consent to Participate** Not applicable.

**Consent for Publication** Not applicable.

**Conflict of Interest** The authors declare no competing interests.

## References

- Phillips DF, Fleischhauer A, Mair A, Walsworth RL (2001) Storage of light in atomic vapor. *Phys Rev Lett* 86:783–786
- Papasimakis N, Fu YH, Fedotov VA, Prosvirnin SL, Tsai DP, Zheludev NI (2009) Metamaterial with polarization and direction insensitive resonant transmission response mimicking electromagnetically induced transparency. *Appl Phys Lett* 94:056613
- Wang JQ, Zhang J, Fan CZ, Mu KJ, Liang EJ, Ding P (2017) Electromagnetic field manipulation in planar nanorod antennas metamaterial for slow light application. *Opt Commun* 383:36–41
- Su H, Wang H, Zhao H, Xue TY, Zhang JW (2017) Liquid-crystal-based electrically tuned electromagnetically induced transparency metasurface switch. *Sci Rep* 7:17378
- Hu FR, Fan YX, Zhang XW, Jiang WY, Chen YZ, Li P, Yin XH, Zhang WT (2018) Intensity modulation of a terahertz bandpass filter: utilizing image currents induced on mems reconfigurable metamaterials. *Opt Lett* 43:17
- Zhang ZD, Wang RB, Zhang ZY, Tang J, Zhang WD, Xue CY, Yan SB (2017) Electromagnetically induced transparency and refractive index sensing for a plasmonic waveguide with a stub coupled ring resonator. *Plasmonics* 12:1007–1013
- Wei ZC, Li XP, Zhong NF, Tan XP, Zhang XM, Liu HZ, Meng HY, Liang RS (2017) Analogue electromagnetically induced transparency based on low-loss metamaterial and its application in nanosensor and slow-light device. *Plasmonics* 12:641–647
- Zheng YL, Chen PP, Ding JY, Yang HM, Nie XF, Zhou XH, Chen XS, Lu W (2018) High intersubband absorption in long-wave quantum well infrared photodetector based on waveguide resonance. *J Phys D Appl Phys* 51:225105
- Zheng YL, Chen PP, Yang HM, Ding JY, Zhou YW, Tang Z, Zhou XH, Li ZF, Li N, Chen XS, Lu W (2019) High-responsivity and polarization-discriminating terahertz photodetector based on plasmonic resonance. *Appl Phys Lett* 114:091105
- Yang H, Li GH, Cao GT, Zhao ZY, Chen J, Ou K, Chen XS, Lu W (2018) Broadband polarization resolving based on dielectric metalenses in the near-infrared. *Opt Express* 26:5632–5643
- Li YL, An BW, Li LZ, Gao J (2018) Broadband LWIR and MWIR absorber by trapezoid multilayered grating and SiO<sub>2</sub> hybrid structures. *Opt Quant Electron* 50:459
- Chen MM, Xiao ZY, Lu XJ, Lv F, Zhou YJ (2019) Simulation of dynamically tunable and switchable electromagnetically induced

- transparency analogue based on metal-graphene hybrid metamaterial. *Carbon* 159:273–282
13. Sun DD, Qi LM (2020) Terahertz polarization-independent electromagnetically -induced transparency structures. *Mod Phys Lett B* 34:2050170
  14. Malik J, Oruganti SK, Song S, Ko NY, Bien F (2018) Electromagnetically induced transparency in sinusoidal modulated ring resonator. *Appl Phys Lett* 112:234102
  15. Petronijevic E, Sibilia C (2016) All-optical tuning of EIT-like dielectric metasurfaces by means of chalcogenide phase change materials. *Opt Express* 24:30411
  16. Chiam SY, Singh R, Rockstuhl C, Lederer F, Zhang WL, Bettiol AA (2009) Analogue of electromagnetically induced transparency in a terahertz metamaterial. *Phys Rev B* 80:153103
  17. Zhang S, Genov DA, Wang Y, Liu M, Zhang X (2008) Plasmon-induced transparency in metamaterials. *Phys Rev Lett* 101:047401
  18. Meng FY, Fu JH, Zhang K, Wu Q, Kim JY, Choi JJ, Lee B, Lee JC (2011) Metamaterial analogue of electromagnetically induced transparency in two orthogonal directions. *J Phys D Appl Phys* 44:265402
  19. Liu N, Langguth L, Weiss T, Kästel J, Fleischhauer M, Pfau T, Giessen H (2009) Plasmonic analogue of electromagnetically induced transparency at the drude damping limit. *Nature Mater* 8:758–762
  20. Jin XR, Park J, Zheng HY, Lee S, Lee YP, Rhee JY, Kim KW, Cheong HS, Jang WH (2011) Highly-dispersive transparency at optical frequencies in planar metamaterials based on two-bright-mode coupling. *Opt Express* 19:21652–21657
  21. Yu W, Meng HY, Chen ZJ, Li XP, Zhang X, Wang FQ, Wei ZC, Tan CH, Huang XG, Li ST (2018) The bright–bright and bright–dark mode coupling-based planar metamaterial for plasmonic EIT-like effect. *Opt Commun* 414:29–33
  22. Wang Q, Ma LY, Cui WL, Chen MD, Zou SL (2019) Ultra-narrow electromagnetically induced transparency in the visible and near-infrared regions. *Appl Phys Lett* 114:213103
  23. He YH, Wang BX, Lou PC, Xu NX, Wang XY, Wang YC (2020) Resonance bandwidth controllable adjustment of electromagnetically induced transparency-like using terahertz metamaterial. *Plasmonics* 15:997–2002
  24. Tang HX, Zhou LJ, Xie JY, Lu LJ, Chen JP (2018) Electromagnetically induced transparency in a silicon self-coupled optical waveguide. *IEEE J Lightwave Technol* 36:2188–2195
  25. He XJ, Ma QX, Jia P, Wang L, Li TY, Wu FM, Jiang JX (2015) Dynamic manipulation of electromagnetically induced transparency with MEMS metamaterials. *Integr Ferroelectr* 161:85–91
  26. Mei J, Shu C, Yang PZ (2019) Tunable electromagnetically induced transparency in graphene metamaterial in two perpendicular polarization directions. *Appl Phys B* 125:130
  27. Duan XY, Chen SQ, Cheng H, Li ZC, Tian JG (2013) Dynamically tunable plasmonically induced transparency by planar hybrid metamaterial. *Opt Lett* 38:483–485
  28. Gu J, Singh R, Liu X, Zhang X, Ma Y, Zhang S, Maier SA, Tian Z, Azad AK, Chen HT (2012) Active control of electromagnetically induced transparency analogue in terahertz metamaterials. *Nat Commun* 3:1151
  29. Schniepp HC, Li JL, McAllister MJ, Sai H, Herrera-Alonso M, Adamson DH, Prud'homme RK, Car R, Saville DA, Aksay IA, (2006) Functionalized single graphene sheets derived from splitting graphite oxide. *J Phys Chem B* 110:8535–8539
  30. Cheng H, Chen SQ, Yu P, Duan XY, Xie BY, Tian JG (2013) Dynamically tunable plasmonically induced transparency in periodically patterned graphene nanostrips. *Appl Phys Lett* 103:36
  31. Zhang HY, Cao YY, Liu YZ, Li Y, Zhang YP (2017) A novel graphene metamaterial design for tunable terahertz plasmon induced transparency by two bright mode coupling. *Opt Commun* 391:9–15
  32. Ning RX, Jiao Z, Bao J (2017) Multi-band and wide-band electromagnetically induced transparency in graphene metasurface of composite structure. *Acta Phys Sin* 12:380
  33. Lundeberg MB, Gao YD, Woessner A, Tan C, Alonso-González P, Watanabe K, Taniguchi T, Hone J, Hillenbrand R, Koppens FH (2017) Thermoelectric detection and imaging of propagating graphene plasmons. *Nature Mater* 16:204–207
  34. Zhu WR, Xiao FJ, Kang M, Sikdar D, Premaratne M (2014) Tunable terahertz left-handed metamaterial based on multi-layer graphene-dielectric composite. *Appl Phys Lett* 104:26
  35. Chen ZH, Tao J, Gu JH, Li J, Hu D, Tan QL, Zhang FC, Huang XG (2016) Tunable metamaterial-induced transparency with gate-controlled on-chip graphene metasurface. *Opt Express* 24:29216
  36. Thongrattanasiri S, Manjavacas A, Abajo F (2012) Quantum finite-size effects in graphene plasmons. *ACS Nano* 6:1766
  37. Zhu L, Fu JH, Meng FY, Ding XM, Dong L, Wu Q (2014) Detuned magnetic dipoles induced transparency in microstrip line for sensing. *IEEE T MAGN* 50:1–4
  38. Chen SH, Pan TS, Peng YY, Yao G, Gao M, Lin Y (2021) Analogue of electromagnetically induced transparency based on bright–bright mode coupling between spoof electric localized surface plasmon and electric dipole. *IEEE T MICROW THEORY* 69–3:1538–1546
  39. Ding J, Arigong B, Ren H, Zhou M, Shao J, Lu M, Chai Y, Lin YK, Zhang HL (2014) Tuneable complementary metamaterial structures based on graphene for single and multiple transparency windows. *Sci Rep* 4:6128
  40. Liu CX, Liu PG, Bian L, Zhou QH, Li GS (2018) Dynamically tunable electromagnetically induced transparency analogy in terahertz metamaterial. *Opt Commun* 19:115102

**Publisher's Note** Springer Nature remains neutral with regard to jurisdictional claims in published maps and institutional affiliations.